Stabilization of an unstable steady state in intracavity frequency-doubled lasers

K. Pyragas,[1,2,*] F. Lange,[1] T. Letz,[1] J. Parisi,[1] and A. Kittel[1]
[1]*Department of Energy and Semiconductor Research, Faculty of Physics, University of Oldenburg, D-26111 Oldenburg*
[2]*Semiconductor Physics Institute, LT-2600 Vilnius, Lithuania*
(Received 30 March 1999; revised manuscript received 17 December 1999)

We predict theoretically that it is possible to stabilize the steady state in multimode, intracavity doubled, diode pumped Nd:YAG (neodymium-doped yttrium aluminum garnet) lasers using two output signals, namely, the sum intensities of the infrared laser modes polarized in two different orthogonal directions (X and Y) and one feedback input parameter, the pump rate. The stabilization is possible for arbitrarily large numbers of modes polarized in the X and Y direction. Different strategies of stabilization based on proportional feedback, derivative control, and their combination are discussed. The analytical and numerical results of the linear control theory are illustrated with numerical simulations of the underlying nonlinear differential equations. We show that one can maintain the stable steady state of the laser output for an arbitrarily large pump rate by taking advantage of a tracking procedure.

PACS number(s): 05.45.Gg

I. INTRODUCTION

We consider a novel approach to the ''green problem'' present in the operation of intracavity frequency-doubled Nd:YAG (neodymium-doped yttrium aluminum garnet) lasers. The Nd:YAG lasers normally emit light at the fundamental wavelength of 1064 nm in the infrared spectral range. By the help of a nonlinear optical crystal such as KTP (potassium titanyl phosphate), one can convert the infrared laser radiation into visible green light (with a wavelength of 532 nm) by the process of second harmonic and sum frequency generation. To obtain the maximum green light output (the intensity of green light produced by the KTP crystal is proportional to the square of the intensity of the fundamental wavelength), the KTP crystal is placed inside the laser cavity. This, however, causes a pronounced dynamical instability in the laser performance. The sum frequency generation provides a nonlinear loss mechanism in the laser dynamics that globally couples the infrared cavity modes, i.e., each infrared cavity mode is coupled to all others. As a result, the output intensity can exhibit periodic and chaotic oscillations.

Such an instability has originally been observed and analyzed by Baer [1]. He developed a deterministic rate equation model, in order to explain the above phenomenon. A detailed linear stability analysis of Baer's equations was performed by Mandel and Wu [2]. One significant advance was made by Oka and Kubota [3] who recognized that the polarization of the cavity modes plays a critical role in the laser dynamics and, therefore, used an intracavity quarter-wave plate to stabilize the laser output. Their theoretical analysis, however, was limited to a model that only includes two orthogonally polarized cavity modes. James *et al.* [4] and Bracikowski and Roy [5] have generalized this model for the case of multiple longitudinal modes. They took into account the birefringence of the YAG crystal and have shown that the modes can exist only in two orthogonal directions of polarization, say, in X and Y directions. For m and n modes polarized in X and Y directions, respectively, this model represents a set of $2(m+n)$ nonlinear coupled rate equations for the mode intensities and gains. The model has successfully predicted the existence of antiphase dynamical states, energy sharing of chaotic polarization modes of the laser, and also the possibility of obtaining stable operation by adjusting the optical axes of the KTP and YAG crystals to a certain angle [5]. Our analysis in the present paper is completely based on that model.

Note that Liu *et al.* [6] have recently developed a more sophisticated model of the laser system that includes both the amplitudes and phases of the electric fields of the infrared light. The previous model [5] is a simplification of this one and can be derived from it by omitting the equations for the phases. Liu *et al.* [6] have shown that the dynamics of the phases can be important in the case that all modes are polarized in the same direction, when the cavity loss due to the emitted green light is extremely small. Because we consider the case of a nonvanishing number of modes in both orthogonal directions and, furthermore, we are interested in high output powers of the green light, we believe that, in our case, the dynamics of the phases does not have a crucial influence.

The main goal of our paper is to show that the laser output can be stabilized by feeding back to the pump rate an amount of the output signal composed of two total intensities of the infrared light polarized in two different orthogonal directions. The underlying idea follows from the linear analysis of the system equations in the vicinity of the fixed point. It is based on the observation that the equations for the total intensities polarized in X and Y directions breaks off from the total system of $2(m+n)$ linear equations describing the dynamics of the individual modes. The problem of the stability of the fixed point reduces to the problem of the stability of the total intensities. The latter is described by a closed system of four linear differential equations. Thus, by feeding back the total intensities, one can effectively control the stability of the steady state. It is possible to achieve and maintain stability for arbitrarily large numbers m and n. For the multimode regime, this is a surprising result, since the system produces hyperchaotic oscillations with multiple posi-

*Electronic address: pyragas@kes0.pfi.lt

 © 2000 The American Physical Society

tive Lyapunov exponents [7]. Stabilization of the fixed point with a single feedback parameter is still possible due to the fact that the fixed point has only two unstable directions, even for a large pump rate, i.e., the fixed point is less unstable than the global strange attractor of the system.

The work of Colet, Roy, and Wiesenfeld [7] was also devoted to a numerical control of chaos in this model. They used the method of occasional proportional feedback [8], in order to stabilize unstable periodic orbits embedded in the chaotic attractor. Another associated work on control of chaos in laser systems was performed by Bielawski *et al.* [9] who managed to stabilize experimentally an unstable steady state in a fiber two-level class B laser.

Our paper is organized as follows. Section II contains the description of the model, the characteristic values of the parameters used in numerical analysis and the model equations in a dimensionless form. In Secs. III and IV, we analyze the steady-state solution of the system and its linear stability, respectively. Section V is devoted to the linear control theory of the steady state. We consider various control strategies based on proportional feedback, derivative control, and their combinations. In the appropriate parameter spaces, we numerically obtain domains of the stable laser operation. Section VI gives an analytical estimation of the parameter values corresponding to the stabilized steady state in the case of proportional feedback control. In Sec. VII, we describe the results of numerical integration of the underlying nonlinear differential equations that confirm the validity of the linear control theory. We discuss a tracking procedure that allows us to maintain the stable steady state for an arbitrarily large pump rate. We finish our paper with conclusions presented in Sec. VIII.

II. MODEL

The dynamics of a multimode Nd:YAG laser with a frequency-doubling KTP crystal located inside the cavity can be described in terms of the rate equations for the intensity I_k and gain G_k associated with each mode [5],

$$\tau_c \frac{dI_k}{dt} = \left(G_k - \alpha_k - g\epsilon I_k - 2\epsilon \sum_{j \neq k} \mu_{jk} I_j \right) I_k , \tag{1a}$$

$$\tau_f \frac{dG_k}{dt} = \Gamma + U(t) - \left(1 + I_k + \beta \sum_{j \neq k} I_j \right) G_k . \tag{1b}$$

Here, $k=1,\ldots,m$ and $k=m+1,\ldots,m+n$ correspond to the modes polarized in X and Y directions, respectively. τ_c means the cavity round trip time and τ_f the fluorescence lifetime of the Nd^{3+} ion. α_k is the cavity loss parameter for the kth mode. β denotes the cross-saturation parameter related to the competition among the different longitudinal modes and is taken to be the same for all mode pairs. The nonlinear coefficient ϵ is associated with the conversion efficiency of the intensity of the infrared intensity into green light converted by the KTP crystal. g gives a geometrical factor that depends on the phase delay due to the YAG and KTP crystals as well as on the angle between the YAG and KTP fast axes. The factor μ_{jk} accounts for the change in geometry when the modes j and k have different polarizations. If the modes have the same polarization $\mu_{jk}=g$, otherwise $\mu_{jk}=1-g$. This factor determines the relative amount of green light produced by second harmonic vs sum frequency generation for different polarization configurations of the laser modes. Γ is a small signal gain related to the pump rate; we consider it as a main control parameter of the system. $U(t)$ is a time-dependent feedback signal introduced to control the stability of the steady state and is experimentally easy to feed back into the system. An explicit expression for that signal will be presented in Sec. V.

In our numerical analysis, we take the same values of the parameters as in the Refs. [5,7]: $\tau_c=0.2$ ns, $\tau_f=240$ μs, $\alpha_k=0.01$ for all $k=1,\ldots,m+n, \beta=0.7$, $\epsilon=5\times10^{-6}$, $g=0.1$. In analytical estimations, we suppose that the parameters can vary, however, their orders remain unchanged.

Equations (1) contain variables and parameters whose magnitude differ from each other by several orders and which have rather different characteristic time scales. To overcome that inconvenience, we rewrite the equations in dimensionless form:

$$I_k' = [\Delta_k + \varepsilon(gI_k - 2M_k)]I_k , \tag{2a}$$

$$\Delta_k' = \gamma + u - [1 + (1-\beta)I_k + \beta(S_x + S_y)](1 + \eta\Delta_k). \tag{2b}$$

The new variables and parameters are defined as follows:

$$\Delta_k = \frac{G_k - \alpha}{G}, \quad \vartheta = \frac{t}{T}, \quad T = \sqrt{\frac{\tau_f \tau_c}{\alpha}}, \quad G = \sqrt{\frac{\alpha \tau_c}{\tau_f}}, \tag{3}$$

$$\varepsilon = \epsilon \sqrt{\frac{\tau_f}{\alpha \tau_c}}, \quad \eta = \sqrt{\frac{\tau_c}{\alpha \tau_f}}, \quad u = \frac{U}{\alpha}, \quad \gamma = \frac{\Gamma}{\alpha}, \tag{4}$$

$$M_k \equiv \sum_{j \neq k} \mu_{jk} I_j + gI_k = gS_x + (1-g)S_y \quad \text{for} \quad k = 1,\ldots,m,$$

$$= gS_y + (1-g)S_x \quad \text{for} \quad k = m+1,\ldots,m+n, \tag{5}$$

$$S_x = \sum_{j=1}^{m} I_j , \quad S_y = \sum_{j=m+1}^{m+n} I_j . \tag{6}$$

I_k' and Δ_k' in Eqs. (2) denote the time derivative of the corresponding variables with respect to the dimensionless time ϑ, $I_k' = dI_k/d\vartheta$ and $\Delta_k' = d\Delta_k/d\vartheta$. For the given values of the parameters, the characteristic time scale T is approximately 2.19 μs. The variable Δ_k describes the deviation of the gain G_k from the cavity loss α normalized to the characteristic scale $G \approx 0.91\times10^{-4}$. The characteristic values of the dimensionless conversion efficiency ε and the square root of the ratio between the inversion and the cavity decay rate η defined in Eq. (4) are $\varepsilon \approx 5.48\times10^{-2}$ and $\eta \approx 9.32\times10^{-3}$. The parameters γ and u are the dimensionless signal gain and feedback signal, respectively, normalized to the cavity loss α. S_x and S_y are the total intensities of the infrared light polarized in X and Y directions, respectively. These parameters are available from experimental measurements. We use them as the feedback variables, in order to stabilize the intensity of the laser.

The variables of Eqs. (2) change in characteristic intervals of the order of unity, and their characteristic time scale is

also of the order of unity. Thus, the above dimensionless form is well suited for numerical as well as analytical analysis.

III. STEADY-STATE SOLUTION

Let us consider the steady-state solutions (fixed points) of Eqs. (2) in the absence of the feedback signal $u=0$. These solutions are defined by the conditions $I_k'=0$, $\Delta_k'=0$, for all $k=1,\ldots,m+n$. The system has multiple fixed points. However, here we do not consider the points for which the intensities of some modes vanish ($I_k=0$ for some k). We restrict our treatment to the symmetrical fixed point for which the intensities and gains among all modes polarized in X and Y directions are identical:

$$I_k \equiv I_x, \quad \Delta_k \equiv \Delta_x, \quad k=1,\ldots,m, \tag{7a}$$

$$I_k \equiv I_y, \quad \Delta_k \equiv \Delta_y, \quad k=m+1,\ldots,m+n. \tag{7b}$$

This fixed point is most important, since it provides the maximum intensity of the green light. Substituting Eqs. (7) into Eqs. (2), we obtain four algebraic equations,

$$\Delta_x - \varepsilon[(2m-1)gI_x + 2n(1-g)I_y] = 0, \tag{8a}$$

$$\Delta_y - \varepsilon[(2n-1)gI_y + 2m(1-g)I_x] = 0, \tag{8b}$$

$$\gamma - \{1+[1+(m-1)\beta]I_x + \beta n I_y\}(1+\eta\Delta_x) = 0, \tag{8c}$$

$$\gamma - \{1+[1+(n-1)\beta]I_y + \beta m I_x\}(1+\eta\Delta_y) = 0 \tag{8d}$$

for four unknown quantities $(I_x, \Delta_x, I_y, \Delta_y)$. Taking into account the smallness of the two parameters ε and η ($\varepsilon, \eta \ll 1$), one can obtain an approximate analytical solution

$$I_x = I + O_2(\varepsilon,\eta), \tag{9a}$$

$$I_y = I + O_2(\varepsilon,\eta), \tag{9b}$$

$$\Delta_x = \varepsilon[(2m-1)g + 2n(1-g)]I + O_3(\varepsilon,\eta), \tag{9c}$$

$$\Delta_y = \varepsilon[(2n-1)g + 2m(1-g)]I + O_3(\varepsilon,\eta), \tag{9d}$$

where

$$I = \frac{\gamma - 1}{1+\beta(m+n-1)} \tag{10}$$

and $O_n(\varepsilon,\eta)$ denotes the nth order corrections with respect to the small parameters ε and η. A more accurate solution can be obtained numerically by an iteration procedure. We start from the solution $I_x = I_y = I$, substitute them in Eqs. (8a) and (8b), and obtain the values of Δ_x and Δ_y. We feed these values in Eqs. (8c) and (8d) and solve the linear system with respect to I_x and I_y. We again put these new values of I_x and I_y into Eqs. (8a) and (8b) and repeat the procedure until all variables converge to the fixed values with a predetermined accuracy. Our algorithm provides a fast convergence to the desired steady-state solution.

The dependence of the steady-state solutions on the signal gain γ obtained from the analytical Eqs. (9) and the iteration procedure of Eqs. (8) for the mode configuration $(m,n)=(1,2)$ are shown in Fig. 1. The analytical estimation [Eqs. (9)] gives a good approximation for the numerical solution of the equation without approximation.

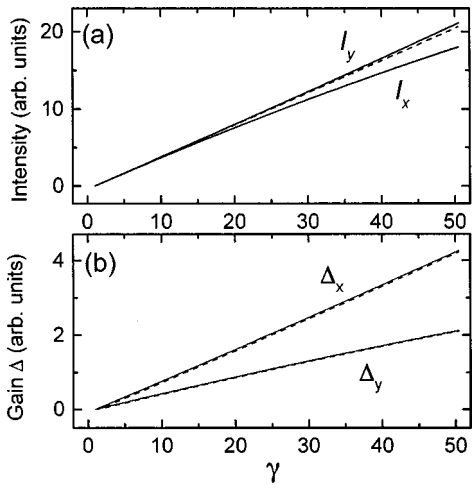

FIG. 1. The steady-state solution of the system [Eqs. (2)] for the mode configuration $(m,n)=(1,2)$. (a) Total mode intensities of the infrared light polarized in X and Y directions, I_x and I_y, respectively, and (b) corresponding normalized mode gains Δ_x and Δ_y as a function of the signal gain γ related to the laser pump rate (considered as the main control parameter). The solid curves display the numerical solutions [Eqs. (8)], the dashed curves the analytical solutions of an approximation [Eqs. (9)].

IV. STABILITY OF THE STEADY STATE

Now, we consider the stability of the steady-state solution. Note that for two specific cases of mode configuration $(m\neq 0, n=0)$ and $(m=n)$, a similar analysis has been performed in Refs. [4,5]. Here, we consider the general case of an arbitrary mode configuration. The linear stability of the steady state is defined by small deviations from the fixed point,

$$(i_k, \delta_k) = (I_k - I_k^0, \Delta_k - \Delta_k^0), \tag{11}$$

where (I_k^0, Δ_k^0) is the steady-state solution defined by Eqs. (8): $(I_k^0, \Delta_k^0) = (I_x, \Delta_x)$ for $k=1,\ldots,m$ and $(I_k^0, \Delta_k^0) = (I_y, \Delta_y)$ for $k=m+1,\ldots,m+n$. Substituting Eq. (11) in Eqs. (2) and performing the standard linearization procedure, one obtains the set of linear equations for small deviations (i_k, δ_k) defining the stability of the fixed point. By excluding the variable δ_k, these equations transform to the form

$$i_k'' + b_x i_k' + c_x i_k + f_x = I_x \delta u, \quad k=1,\ldots,m, \tag{12a}$$

$$i_k'' + b_y i_k' + c_y i_k + f_y = I_y \delta u, \quad k=m+1,\ldots,m+n, \tag{12b}$$

where δu is the linearized feedback signal. The coefficients b_x and c_x in Eq. (12a) are

$$b_x = \frac{\eta\gamma}{1+\eta\Delta_x} - \varepsilon g I_x, \tag{13a}$$

$$c_x=\left[(1-\beta)(1+\eta\Delta_x)-\frac{\varepsilon\eta g\gamma}{1+\eta\Delta_x}\right]I_x, \tag{13b}$$

and f_x is a linear homogeneous function of the variables s_x, s_y and their time derivatives

$$f_x=\beta(1+\eta\Delta_x)I_x(s_x+s_y)+\frac{2\varepsilon\eta\gamma}{1+\eta\Delta_x}I_x[gs_x+(1-g)s_y] +2\varepsilon I_x[gs_x'+(1-g)s_y',], \tag{14}$$

where s_x and s_y define the deviation of the sum intensities

$$s_x=\sum_{j=1}^{m} i_j, \quad s_y=\sum_{j=m+1}^{m+n} i_j. \tag{15}$$

The expressions for the coefficients b_y and c_y in Eq. (12b) can be obtained from Eqs. (13a) and (13b), respectively, by replacing the subscript x by y. The function f_y results from Eq. (14) by interchanging the subscript x and y.

The coefficients a_x, b_x, a_y, and b_y in Eqs. (12) are independent of the index k, as well as f_x and f_y are linear functions of the sums s_x and s_y. These features allow us to derive the closed system of equations for the sums s_x and s_y. Those equations are simply extracted by summing Eq. (12a) through all X modes (from $k=1$ to $k=m$) and Eq. (12b) through all Y modes (from $k=m+1$ to $k=m+n$):

$$s_x''+b_xs_x'+c_xs_x+mf_x=mI_x\delta u, \tag{16a}$$

$$s_y''+b_ys_y'+c_ys_y+nf_y=nI_y\delta u. \tag{16b}$$

Taking into account the expressions for f_x [Eq. (14)] and f_y, Eqs. (16) can be rewritten in a more convenient form,

$$s_x''+B_xs_x'+C_xs_x+E_xs_y'+F_xs_y=mI_x\delta u, \tag{17a}$$

$$s_y''+B_ys_y'+C_ys_y+E_ys_x'+F_ys_x=nI_y\delta u. \tag{17b}$$

The coefficients B_x, C_x, E_x, and F_x in Eq. (17a) are

$$B_x=\frac{\eta\gamma}{1+\eta\Delta_x}+\varepsilon g(2m-1)I_x, \tag{18a}$$

$$C_x=\left\{[1+(m-1)\beta](1+\eta\Delta_x)+(2m-1)\frac{\varepsilon\eta g\gamma}{1+\eta\Delta_x}\right\}I_x, \tag{18b}$$

$$E_x=2\varepsilon(1-g)mI_x, \tag{18c}$$

$$F_x=\left[\beta(1+\eta\Delta_x)+2(1-g)\frac{\varepsilon\eta g\gamma}{1+\eta\Delta_x}\right]mI_x. \tag{18d}$$

The expressions for the coefficients B_y, C_y, E_y, and F_y in Eq. (17b) are obtained from Eqs. (18a), (18b), (18c), and (18d), respectively, by replacing the subscript x by y and the number m by n.

In this section, we consider the problem of stability of the steady state in the absence of the feedback signal $\delta u=0$. In this case, the right-hand side (rhs) of Eqs. (12) and (17) are zeros. The problem of stability is completely defined by Eqs. (12) that describe the dynamics of small perturbations in an $R^{2(m+n)}$ dimensional phase space defined by the variables $(i_1,\ldots,i_{m+n},i_1',\ldots,i_{m+n}')$. The origin of this space is stable, if the real parts of all $2(m+n)$ eigenvalues of Eqs. (12) are negative. For a large number of modes, the eigenvalue problem for the system (12) is not a trivial one. However, it can be essentially simplified due to the fact that, for the sums s_x and s_y, it is possible to split off Eqs. (17) from the total system of Eqs. (12).

The problem can be divided into two much more simple ones. The first consists of the analysis of Eqs. (17) for the sums s_x and s_y. The origin $(s_x,s_y,s_x',s_y')=0$ of these equations defines some subspace $R^{2(m+n)-4}$ in the original phase space $R^{2(m+n)}$, $R^{2(m+n)-4}\subset R^{2(m+n)}$. The stability of this subspace is determined by four eigenvalues (Λ_i, $i=1,\ldots,4$) of Eqs. (17). Obviously, these four eigenvalues are the eigenvalues of the original Eqs. (12) as well. The second problem consists of determining the remaining $2(m+n)-4$ eigenvalues $\lambda_i, i=1,\ldots,2(m+n)-4$ of Eqs. (12) that define the stability of the trajectories inside the subspace $(s_x,s_y,s_x',s_y')=0$. In this subspace, $f_x=f_y=0$ and Eqs. (12) transform to

$$i_k''+b_xi_k'+c_xi_k=0, \quad k=1,\ldots,m, \tag{19a}$$

$$i_k''+b_yi_k'+c_yi_k=0, \quad k=m+1,\ldots,m+n. \tag{19b}$$

The system of Eqs. (12) splits into a set of $2(m+n)$ independent equations. There are m identical Eqs. (19a) for the X polarization and n identical Eqs. (19b) for the Y polarization. As a result, system (19) has only four different eigenvalues, two of them, $\lambda_{(1,2)}^{(x)}$, correspond to the X polarization and the other two, $\lambda_{(1,2)}^{(y)}$, to the Y polarization. Thus, for a large number of modes, the eigenvalues of the original system (12) are highly degenerated. For any $m>1$ and $n>1$, the system has only eight different eigenvalues, four of them are defined by Eqs. (17) and the remaining four by Eqs. (19). Now we discuss the above two problems in detail.

Let us start with the first problem, i.e., consider the stability of Eqs. (17). The eigenvalues Λ_i of this system are determined by the characteristic equation

$$\det\begin{pmatrix}\Lambda^2+B_x\Lambda+C_x & E_x\Lambda+F_x\\ E_y\Lambda+F_y & \Lambda^2+B_y\Lambda+C_y\end{pmatrix}=0 \tag{20}$$

that represents the fourth-order polynomial

$$\Lambda^4+a_1\Lambda^3+a_2\Lambda^2+a_3\Lambda+a_4=0, \tag{21}$$

where

$$a_1=B_x+B_y, \tag{22a}$$

$$a_2=C_x+C_y+B_xB_y-E_xE_y, \tag{22b}$$

$$a_3=B_yC_x+B_xC_y-E_yF_x-E_xF_y, \tag{22c}$$

$$a_4=C_xC_y-F_xF_y. \tag{22d}$$

The origin of system (17) is stable, if the real parts of all roots of the polynomial (21) are negative. The numerical solution of Eq. (21) is illustrated in Fig. 2(a). The dependence of the eigenvalues Λ_i on the signal gain γ for the

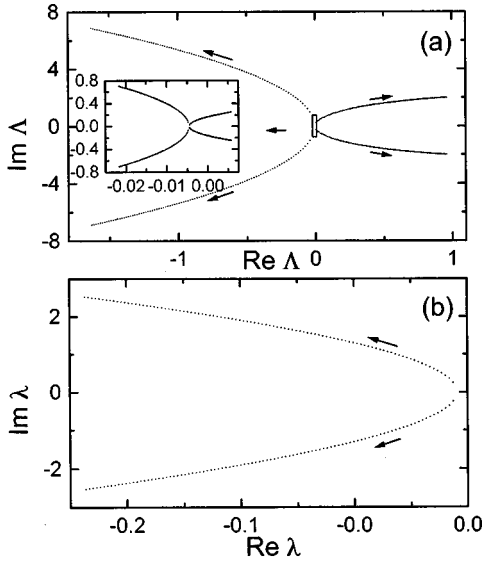

FIG. 2. Evolution of eigenvalues of the fixed point in the complex plane, when the signal gain γ is increased from 1 to 50 with the step 0.5. The arrows show directions corresponding to the increase of γ. The mode configuration is (1,2). (a) Eigenvalues defined by Eqs. (21). (b) Eigenvalues defined by Eqs. (23). The insert in (a) shows an enlarged region close to the origin. Here γ is increased from 1 to 1.5 with the step 0.005.

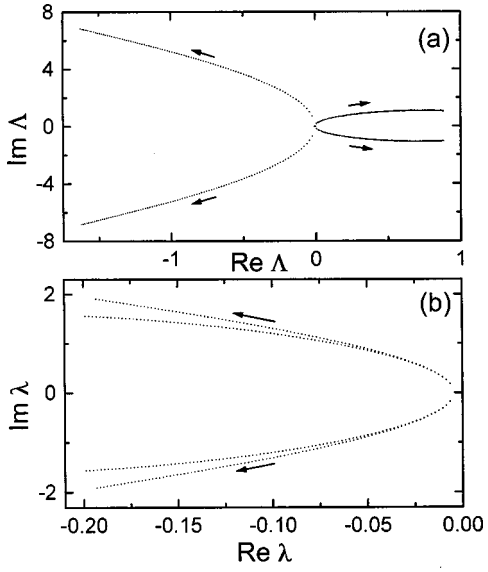

FIG. 3. The same as in Fig. 2 but for the mode configuration (2,4).

mode configuration $(m,n)=(1,2)$ is shown in the complex plane. At $\gamma=\gamma_c\approx 1.22$, the real part of two complex conjugated eigenvalues becomes positive. The fixed point loses its stability through a Hopf bifurcation. Two other complex conjugated eigenvalues have a negative real part for any γ.

Next, we consider the second problem, the stability of the trajectories in the subspace $(s_x,s_y,s_x',s_y')=0$. That problem is defined by Eqs. (19). The four different eigenvalues λ_i are obtained from the two characteristic equations $\lambda^2+b_x\lambda+c_x=0$ and $\lambda^2+b_y\lambda+c_y=0$ that can be solved explicitly:

$$\lambda_{1,2}^{(x)}=-\frac{b_x}{2}\pm\sqrt{\frac{b_x^2}{4}-c_x}, \tag{23a}$$

$$\lambda_{1,2}^{(y)}=-\frac{b_y}{2}\pm\sqrt{\frac{b_y^2}{4}-c_y}. \tag{23b}$$

The real parts of these eigenvalues are negative at the conditions

$$c_x>0, \quad c_y>0, \quad b_x>0, \quad b_y>0. \tag{24}$$

Let us evaluate these inequalities for the case of a vanishing conversion efficiency and vanishing ratio between the inversion and cavity relaxation rate $(\varepsilon,\eta\to 0)$. We have $c_x\approx c_y\approx(1-\beta)I$ and $b_x\approx b_y\approx\eta\gamma-\varepsilon g I$. Thus, c_x and c_y are positive, if $\beta<1$ and b_x and b_y are positive (for $\gamma\gg 1$), if $g<\eta/\varepsilon[1+\beta(m+n-1)]$. For the given values of the parameters, these conditions are fulfilled and, hence, the system is stable in the subspace $(s_x,s_y,s_x',s_y')=0$.

Figure 2(b) illustrates the dependence of the eigenvalues $\lambda_{1,2}^{(y)}$ on γ for the mode configuration (1,2). As it is expected, the real parts of these eigenvalues are negative for all values of γ. Note that, for this mode configuration, the system has only one pair of complex conjugated eigenvalues $(\lambda_{1,2}^{(y)})$ corresponding to the subspace $(s_x,s_y,s_x',s_y')=0$. For $m=1$, Eq. (19a) is automatically satisfied, since we have $s_x\equiv i_1$ and $s_x=0$ in the subspace. The total number of eigenvalues in this case is six; four of them are defined by Eqs. (17) and two by Eq. (19b).

For any mode configuration (m,n), the evolution of the eigenvalues in the complex plane is similar to that presented in Fig. 2. Figure 3 shows such an evolution for the mode configuration (2,4). The only difference is that the number of different eigenvalues in the subspace $(s_x,s_y,s_x',s_y')=0$ is now four. They all have negative real parts. Again, only two eigenvalues corresponding to the dynamics of the sums s_x and s_y [Eqs. (17)] become positive when γ exceeds some threshold value. Note that the total number of eigenvalues in this case is 12 and only eight of them are different. This means that the eigenvalues corresponding to the subspace $(s_x,s_y,s_x',s_y')=0$ are degenerated.

In conclusion of this section, we emphasize an important feature discovered in our analysis. For any mode configuration (m,n), the unstable fixed point has only two unstable eigenvalues, even for a large signal gain γ. These eigenvalues correspond to the dynamics of the sum intensities s_x and s_y, and, hence, they should be effectively controlled by feeding back into the system a signal composed of these intensities. We consider that control procedure in the next section.

V. LINEAR CONTROL THEORY

Now, we analyze the stability of the steady state in the case of a nonvanishing feedback signal, $\delta u\neq 0$. We combine this signal from the sum intensities S_x and S_y [Eq. (6)] of the infrared light polarized in two orthogonal directions, X and Y, respectively. These intensities are available from experimental observation. The feedback signal does not have to change the position of the fixed point. We look at the following general form of the feedback signal satisfying the above main requirement:

$$U = K_x(S_x - S_x^0) + K_y(S_y - S_y^0) + D_x\frac{dS_x}{dt} + D_y\frac{dS_y}{dt}, \tag{25}$$

where K_x, K_y, D_x, and D_y are the feedback gain coefficients, $S_x^0 = mI_x$ and $S_y^0 = nI_y$ the steady-state values of the sum intensities. In the dimensionless form [Eq. (2)], the feedback signal is

$$u = k_x(S_x - S_x^0) + k_y(S_y - S_y^0) + d_x S_x' + d_y S_y', \tag{26}$$

where $k_x = K_x/\alpha$, $k_y = K_y/\alpha$, $d_x = D_x/T\alpha$, and $d_y = D_y/T\alpha$. Linearization of Eq. (26) in the vicinity of the fixed point leads to

$$\delta u = k_x s_x + k_y s_y + d_x s_x' + d_y s_y'. \tag{27}$$

Next, we reconsider Eqs. (12) and (17) by taking into account Eq. (27). We first note that Eqs. (19) that describe the stability of the trajectories in the subspace $(s_x, s_y, s_x', s_y') = 0$ remain unchanged in the presence of the feedback signal (27). This holds because the feedback signal (27) is a linear homogeneous function of the variables (s_x, s_y, s_x', s_y'), and it vanishes in the subspace $(s_x, s_y, s_x', s_y') = 0$. Thus, the feedback signal does not change the eigenvalues (23) associated with the stability of the trajectories in the subspace $(s_x, s_y, s_x', s_y') = 0$. The trajectories in the subspace are stable in the absence of the feedback signal, and, hence, they remain stable in the presence of the feedback signal (27). The feedback only influences the eigenvalues Λ_i associated with Eqs. (17) that describe the stability of the sums s_x and s_y.

In the presence of the feedback signal (27), Eqs. (17) take the form

$$s_x'' + \tilde{B}_x s_x' + \tilde{C}_x s_x + \tilde{E}_x s_y' + \tilde{F}_x s_y = 0, \tag{28a}$$

$$s_y'' + \tilde{B}_y s_y' + \tilde{C}_y s_y + \tilde{E}_y s_x' + \tilde{F}_y s_x = 0, \tag{28b}$$

where

$$\tilde{B}_x = B_x - d_x m I_x, \tag{29a}$$

$$\tilde{C}_x = C_x - k_x m I_x, \tag{29b}$$

$$\tilde{E}_x = E_x - d_y m I_x, \tag{29c}$$

$$\tilde{F}_x = F_x - k_y m I_x. \tag{29d}$$

The expressions for the coefficients $\tilde{B}_y$, $\tilde{C}_y$, $\tilde{E}_y$, and $\tilde{F}_y$ in Eq. (28b) are obtained from Eqs. (29a), (29b), (29c), and (29d), respectively, via replacing the subscript x by y and the number m by n.

The characteristic equation of the system (28) is defined by the polynomial

$$\Lambda^4 + \tilde{a}_1\Lambda^3 + \tilde{a}_2\Lambda^2 + \tilde{a}_3\Lambda + \tilde{a}_4 = 0, \tag{30}$$

where

$$\tilde{a}_1 = \tilde{B}_x + \tilde{B}_y, \tag{31a}$$

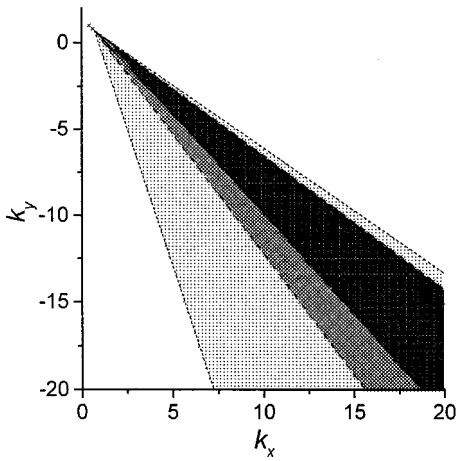

FIG. 4. The domains of stability in the (k_x, k_y) parameter plane obtained for proportional feedback control at different values of the signal gain γ (1.4, 2, 50). The darker regions correspond to the larger values of γ. The lines indicate the domain boundaries, analytically estimated in Sec. VI [Eq. (35)]. The mode configuration is (1,2).

$$\tilde{a}_2 = \tilde{C}_x + \tilde{C}_y + \tilde{B}_x\tilde{B}_y - \tilde{E}_x\tilde{E}_y, \tag{31b}$$

$$\tilde{a}_3 = \tilde{B}_y\tilde{C}_x + \tilde{B}_x\tilde{C}_y - \tilde{E}_y\tilde{F}_x - \tilde{E}_x\tilde{F}_y, \tag{31c}$$

$$\tilde{a}_4 = \tilde{C}_x\tilde{C}_y - \tilde{F}_x\tilde{F}_y. \tag{31d}$$

We use the Hurwitz criterion [10], in order to analyze the stability of the system under control. According to that criterion, all roots of the fourth-order polynomial (30) have negative real parts, if there are satisfied the four inequalities

$$\tilde{a}_1 > 0, \quad \tilde{a}_3 > 0, \quad \tilde{a}_4 > 0, \quad \tilde{a}_3(\tilde{a}_1\tilde{a}_2 - \tilde{a}_3) - \tilde{a}_4\tilde{a}_1^2 > 0. \tag{32}$$

For different control strategies, we have checked these inequalities numerically. The feedback signal (27) depends on four parameters (k_x, k_y, d_x, d_y) that define a four-dimensional control vector in a suitable parameter space. We restricted our consideration to three different types of the two-parameter control (i.e., two of four components in the control vector were taken to be zeros), namely, (a) the proportional feedback control $(k_x, k_y, 0, 0)$, (b) the derivative control $(0, 0, d_x, d_y)$, and (c) the combined control $(k_x, 0, d_x, 0)$ or $(0, k_y, 0, d_y)$ by using only one output of *X*- or *Y*-polarized infrared light. Below, we discuss the results of the numerical analysis obtained for these different control strategies.

(a) The results of proportional feedback control for the mode configuration (1,2) are shown in Fig. 4. In the plane of the feedback parameters (k_x, k_y), the domains of stability are shown for different values of the signal gain γ. The darker regions correspond to the larger γ. With increasing γ, the relative area of the stability domain decreases, however, it remains infinitely large for any large γ. To stabilize the system, the feedback has to be positive $(k_x > 0)$ for the *X* polarization (there is only one mode in this direction, $m = 1$) and negative $(k_y < 0)$ for the *Y* polarization (there are two modes in this direction, $n = 2$). In other words, the feedback has to

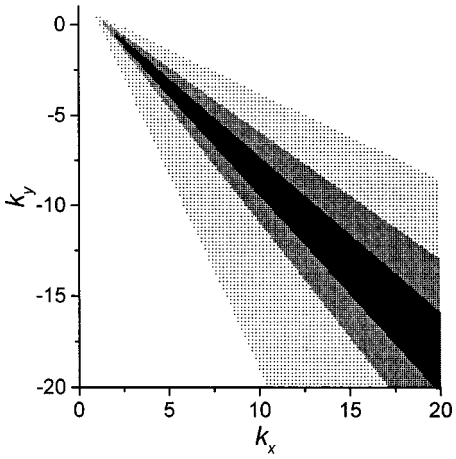

FIG. 5. The domains of stability in the (k_x,k_y) parameter plane obtained for proportional feedback control at fixed $\gamma=50$ and different mode configurations (1,4), (2,4), (3,4). The darker regions correspond to the larger values of m.

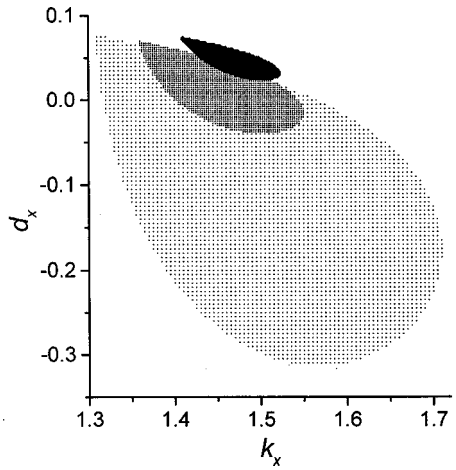

FIG. 7. The domains of stability in the (k_x,d_x) parameter plane obtained for combined control $(k_x,0,d_x,0)$ at different values of the signal gain γ (5, 20, 50). The darker regions correspond to the larger values of γ. The mode configuration is (1,2).

try to restore the symmetry in the asymmetric distribution of the outputs in the X and Y directions; it has to increase the output intensity in the direction where the number of modes is small and decrease the output intensity in the direction where the number of modes is large. Such an observation seems to be general for any mode configuration (m,n). For any $m<n$, the domain of stability is basically located in the region $k_x>0$, $k_y<0$. In the symmetrical case $m=n$, there remains no domain of stability. Figure 5 shows the dependence of the stability domain on the mode configuration (m,n). Here, n is fixed equal to 4 and m is varied from 1 to 4. With increasing m, the stability domain decreases and, finally, disappears when $m=n=4$. Thus only asymmetric mode configurations $(m\neq n)$ are controllable.

(b) The derivative feedback control is illustrated in Fig. 6. The domains of stability are shown in the plane of control parameters (d_x,d_y) for the fixed mode configuration (1,2) and different values of the signal gain γ. Here, the darker regions correspond to the smaller γ. With increasing γ, the stability domain moves towards the origin of the (d_x,d_y) plane. The feedback has to be positive $(d_x>0)$ for the X polarization and negative $(d_y<0)$ for the Y polarization, as well as in the case of proportional feedback control.

(c) The combined feedback control strategies $(k_x,0,d_x,0)$ and $(0,k_y,0,d_y)$ for the mode configuration (1,2) and different values of the signal gain γ are illustrated in Figs. 7 and 8, respectively. In both cases, there are only finite area domains of stability that decrease with increasing γ and disappear for sufficiently large γ. Thus, these control strategies are not so efficient as those considered in (a) and (b), i.e., control with two output signals corresponding to different directions of polarization is much more efficient than is the case for control that uses the output of only one direction of polarization.

Note that none of the above techniques does work for the symmetrical case $m=n$. In our model, all X modes and all Y modes have identical parameters. In Sec. VII, we show that the symmetrical case can be stabilized if this identity is destroyed.

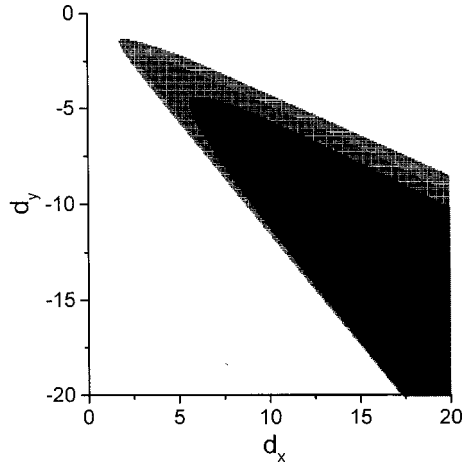

FIG. 6. The domains of stability in the (d_x,d_y) parameter plane obtained for derivative control technique at different values of the signal gain γ (2, 5, 50). The darker regions correspond to the smaller values of γ. The mode configuration is (1,2).

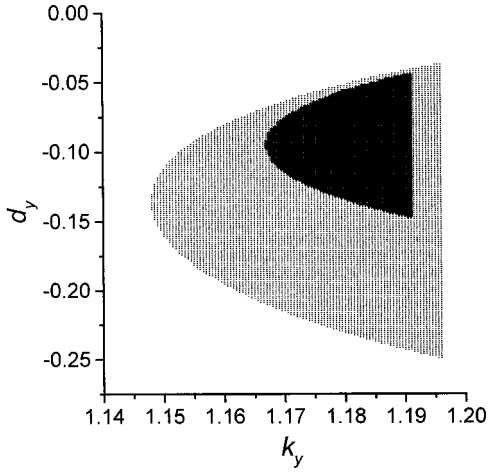

FIG. 8. The domains of stability in the (k_y,d_y) parameter plane obtained for combined control $(0,k_y,0,d_y)$ at different values of the signal gain γ (5, 10, 20). The darker regions correspond to the larger values of γ. The mode configuration is (1,2).

Both the proportional feedback and the derivative control techniques have infinitely large area domains of stability in the appropriate parameter spaces. However, the derivative control method may be sensitive to noise, since it requires an experimental differentiation of the output signal. Most appropriate for experimental applications, therefore, is the proportional feedback technique. To get more insight into that method, we perform some analytical estimations in Sec. VI.

VI. ANALYTICAL ESTIMATIONS

In order to find analytical expressions for the boundaries of the stability domain, we evaluate the inequalities (32) in the limit of $\varepsilon, \eta \to 0$. Here we restrict our analysis to the case of the proportional feedback technique, representing the most promising alternative for experimental applications. Similar estimations can be performed for the other methods as well.

Expanding the parameters $\tilde{a}_1$, $\tilde{a}_3$, $\tilde{a}_4$, and $\tilde{a}_3(\tilde{a}_1\tilde{a}_2 - \tilde{a}_3) - \tilde{a}_4\tilde{a}_1^2$ in a power series of the parameters ε and η, we end up with

$$\tilde{a}_1 = 2[\gamma\eta + \varepsilon(m+n-1)gI] + O_3(\varepsilon,\eta), \tag{33a}$$

$$\tilde{a}_3 = [p_x^{(1)}(k_x-\beta) + p_y^{(1)}(k_y-\beta)]I^2\varepsilon + O_3(\varepsilon,\eta), \tag{33b}$$

$$\tilde{a}_4 = [1+\beta(m+n-1) - mk_x - nk_y](1-\beta)I^2 + O_2(\varepsilon,\eta), \tag{33c}$$

$$\begin{aligned}\tilde{a}_3(\tilde{a}_1\tilde{a}_2 - \tilde{a}_3) - \tilde{a}_4\tilde{a}_1^2 &= -[p_x^{(1)}(k_x-\beta) + p_y^{(1)}][p_x^{(2)}(k_x-\beta) + p_y^{(2)}]I^4\varepsilon^2 \\ &\quad + O_4(\varepsilon,\eta),\end{aligned} \tag{33d}$$

where

$$p_x^{(1)} = m\left[2n - g(4n-1) - \frac{\eta\gamma}{\varepsilon I}\right], \tag{34a}$$

$$p_y^{(1)} = n\left[2m - g(4m-1) - \frac{\eta\gamma}{\varepsilon I}\right], \tag{34b}$$

$$p_x^{(2)} = m\left[2n - g(1+2n-2m) + \frac{\eta\gamma}{\varepsilon I}\right], \tag{34c}$$

$$p_y^{(2)} = n\left[2m - g(1+2m-2n) + \frac{\eta\gamma}{\varepsilon I}\right]. \tag{34d}$$

According to the conditions (32), the fixed point is stable if all four parameters in Eqs. (33) are positive. In approximation of the leading ε and η terms all these parameters are positive, if the following two inequalities are satisfied:

$$p_x^{(1)}(k_x-\beta) + p_y^{(1)}(k_y-\beta) > 0, \tag{35a}$$

$$p_x^{(2)}(k_x-\beta) + p_y^{(2)}(k_y-\beta) < 0. \tag{35b}$$

These inequalities define the stability domain in the (k_x,k_y) parameter plane. The domain is paled by the two lines $k_x - \beta = b_1(k_y-\beta)$ and $k_x-\beta = b_2(k_y-\beta)$ that cross at the point $(k_x,k_y)=(\beta,\beta)$ and have the slope coefficients $b_1 = -p_y^{(1)}/p_x^{(1)}$ and $b_2 = -p_y^{(2)}/p_x^{(2)}$. These lines are shown in Fig. 4 for the mode configuration (1,2) and different values of the signal gain γ. The lines give a good quantitative estimation of the domain boundaries.

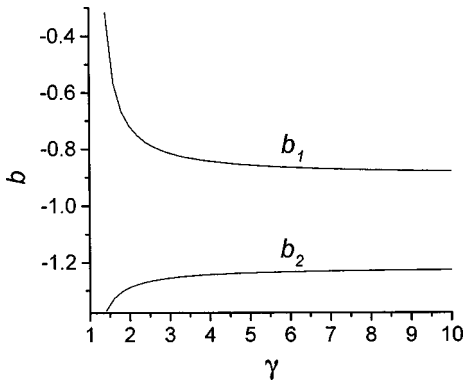

FIG. 9. The slope coefficients $b_1 = -p_y^{(1)}/p_x^{(1)}$ and $b_2 = -p_y^{(2)}/p_x^{(2)}$ of the lines defining the boundaries of the control domain [Eqs. (35)] vs signal gain γ for the mode configuration (1,2).

The above analytical result allows us to easily analyze the dependence of the stability domain on the signal gain γ. Figure 9 illustrates that dependence for the mode configuration (1,2). There are shown the slopes $b_1(\gamma)$ and $b_2(\gamma)$ of the lines defining the boundaries of the stability domain. For small values of γ, these slopes considerably differ from each other, and the stability domain occupies a large part of the (k_x,k_y) plane. With increasing γ the difference between the slopes decreases, however, it remains finite when $\gamma \to \infty$. The latter guarantees the theoretical possibility of stabilizing the steady state for an arbitrarily large pump rate. The result is valid for an arbitrary mode configuration (m,n), provided $m \neq n$. For $m=n$, the slopes coincide, $b_1(\gamma) = b_2(\gamma)$, at any γ, and the stability domain disappears. This finding gives an analytical explanation why symmetrical mode configurations are uncontrollable.

From Fig. 9 it is obvious that the slopes satisfy the inequality $b_2(\gamma) < -1 < b_1(\gamma)$ for any γ with the value -1 located approximately in the center between $b_2(\gamma)$ and $b_1(\gamma)$. Thus, a good choice of the parameters (k_x,k_y) is the one that lies close to the line $k_x - \beta = -(k_y-\beta)$ having a negative unity slope coefficient. Knowledge of such a relationship between the parameters k_x and k_y can be useful for an experimental search of the stability domain in the (k_x,k_y) plane. For any γ stabilization is possible for any (k_x,k_y) lying in the domain $b_1(\infty)(k_y-\beta) < k_x - \beta < b_2(\infty)(k_y-\beta)$ and especially for the line $k_x-\beta = -(k_y-\beta)$. Thus, one can fix the parameters (k_x,k_y) in that domain and track the steady state from a region of small signal gain γ (where the fixed point is stable without feedback) to the region of large signal gain. The tracking procedure will be considered in Sec. VII.

VII. TRACKING THE STEADY STATE

We have verified numerically the linear control theory by integrating the system of nonlinear differential equations (2). We applied the fourth-order Runge-Kutta method [11] with

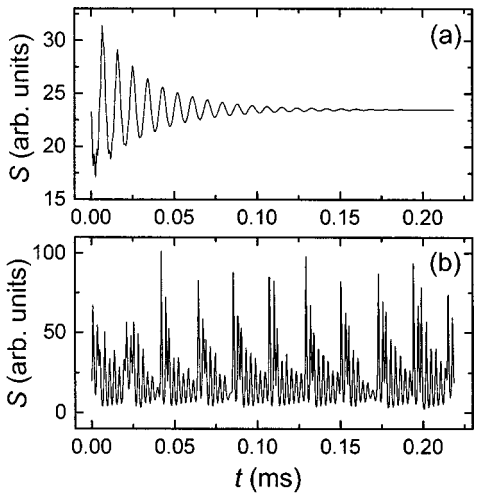

FIG. 10. The dynamics of the total intensity $S=S_x+S_y$ of the infrared light for proportional feedback control determined by the numerical solution of Eqs. (2). The mode configuration is (1,2). The parameter values are $\gamma=20$, $k_x=10$, $k_y=-8.6$, $S_x^0=I_x \approx 7{,}539$, $S_y^0=2I_y\approx 2\times 7.979$, and $u_m=10$. (a) and (b) correspond to initial conditions chosen close and far away from the steady-state solution, respectively.

the fixed time step $h=0.02$. The numerical analysis shows that the linear theory correctly predicts the stability domains for different control strategies. Figure 10 illustrates an example of the system dynamics, time series of the total intensity $S=S_x+S_y$ of the infrared light, in the case of proportional feedback control for the mode configuration (1,2) and the signal gain $\gamma=20$. The control parameters $(k_x,k_y)=(10,-8.6)$ are chosen on the line $k_x-\beta=-(k_y-\beta)$. To avoid large values of the feedback signal the perturbation u has been restricted in the following way. For $|u|<u_m$ with u_m representing some predetermined maximum value, the perturbation has been calculated from Eq. (26). When u exceeded the maximum (u_m) or minimum value $(-u_m)$, we ascribed it to u_m or $-u_m$, respectively.

The asymptotic dynamics essentially depends on the initial conditions. If the initial conditions are close to the fixed point, the feedback perturbation stabilizes the steady state [Fig. 10(a)]. If the perturbation is switched on, when the initial conditions lie on the strange attractor of the uncontrolled system, the perturbation cannot stabilize the steady state [Fig. 10(b)]. This is because the trajectories belonging to the strange attractor are far away from the fixed point and the fixed point has only a finite domain of attraction in phase space.

In order to overcome that problem, one can use the tracking procedure. Here, we switch on the feedback perturbation at a low signal gain γ corresponding to a stable steady state of the unperturbed system and then increase it slowly to a desired level. If the rate of varying γ is slower than a characteristic transient rate of the steady state, the system adiabatically follows the changes of γ by remaining inside the stability regime of the steady state. Due to the existence of the universal (for any γ) stability domain in the (k_x,k_y) plane, the parameters k_x and k_y can be fixed during the tracking procedure.

Figure 11 illustrates the tracking of the steady state for the

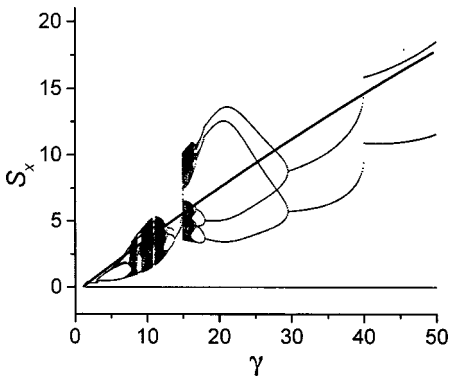

FIG. 11. The bifurcation diagram of the system for the mode configuration (1,2) obtained in the absence of the feedback signal. The minima of intensity S_x are plotted vs the signal gain γ. The thick solid line indicates the stabilized steady state obtained by the tracking procedure. The values of the parameters are $k_x=10$, $k_y=-8.6$, $u_m=10$, and $\omega_c=0.01$.

mode configuration (1,2). The solid line corresponds to the stabilized steady state. The points describe the bifurcation diagram of the uncontrolled system. They show an evolution of the minima of the S_x signal under the increase of γ. In the absence of the feedback signal, the system experiences periodic as well as chaotic oscillations. The tracking procedure allows us to keep the system on the originally unstable steady state for an arbitrarily large signal gain γ. In order to take our simulations as a more accurate approach to a real experimental situation, we have applied a slightly modified proportional feedback method [12]. A low-pass filter was incorporated in the feedback loop, to provide an automatic search of the steady-state values S_x^0 and S_y^0 that are required for the original proportional feedback technique. The filter produces an additional degree of freedom defined by the differential equation

$$z'=\omega_c(k_xS_x+k_yS_y-z), \tag{36}$$

where $\omega_c=0.01$ gives the characteristic cutoff frequency. The output of the filter is taken as the feedback signal

$$u=k_xS_x+k_yS_y-z. \tag{37}$$

The filter tends to adapt the z variable to the steady state of the system, $z=k_xS_x^0+k_yS_y^0$. At $\omega_c\to 0$ the present method becomes close to the conventional proportional feedback technique with the obvious advantage that it does not require knowledge of the steady-state values S_x^0 and S_y^0 [12]. Due to its adaptive features, our technique can be successfully applied, even in the case of a slow drift of the system parameters.

Note that the linear analysis of the system presented in Secs. IV, V, and VI is performed under the assumption of identical parameters of the different modes. As a consequence, we have been able to simplify the stability problem by separately looking at the dynamics of the sums s_x and s_y and the dynamics of the system in the subspace $(s_x,s_y,s_x',s_y')=0$. The identity of the modes is responsible for the degeneration of the eigenvalues of the fixed point. In real laser systems, however, the parameters of the modes are slightly different. These circumstances destroy the symmetry

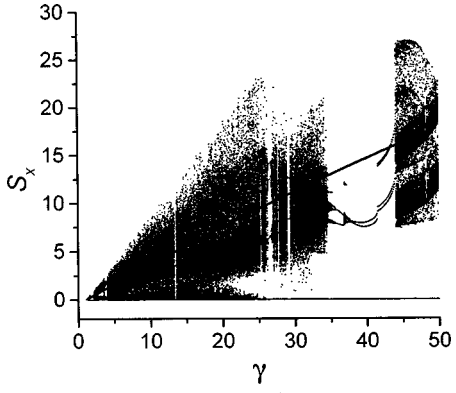

FIG. 12. The same as in Fig. 11, but the parameters of the modes are not identical. The factor μ_{jk} is scattered randomly by 20% around the constant values ($\mu_{jk}=g$ and $\mu_{jk}=1-g$ for parallel modes and otherwise, respectively) taken in the previous consideration.

of the system and abolish the degeneration of the eigenvalues. The question arises, how sensitive is the stabilization procedure with regard to a small scattering of the mode parameters. To answer that question we have analyzed the problem numerically. Figure 12 displays the bifurcation diagram and the steady state stabilized by the tracking procedure in the case of a randomly scattered factor μ_{jk}. Any difference between the mode parameters leads to a more complicated bifurcation diagram compared to that presented in Fig. 12. There are more chaotic and high-periodic states compared to the case of identical modes, however, the tracking procedure still works. Stabilization of the steady state is possible even for a rather large scattering of the factor μ_{jk} reaching 50%. Similar results have been observed upon scattering other parameters of the modes. So far, the results of Secs. IV, V, and VI are only weakly sensitive to a small scattering of the mode parameters.

In Secs. V and VI, we have demonstrated that the symmetric mode configurations ($m=n$) are uncontrollable. However, they may become controllable, if we take into account the nonidentity of the mode parameters. The linear analysis in Secs. V and VI has been performed for fixed numbers m and n. In a real experimental situation, the number of modes changes with increasing the pump rate. This is because the different modes have different signal gains γ. To model that finding, we simply have replaced γ by $p\,\gamma_k$ in Eq. (2), where p describes the pump rate. For the initial mode configuration (2,2) and different values of γ_k, the bifurcation diagram of the system as a function of the pump rate p is shown in Fig. 13(a). The solid curve corresponds to the stabilized steady state attained by the tracking procedure. Figure 13(b) illustrates the dependence of the stabilized individual mode intensities on the pump rate p. I_1 and I_2 relate to the X polarization, I_3 and I_4 to the Y polarization. With increasing p, there first appear the Y-polarized modes that have larger signal gains ($\gamma_4=1$, $\gamma_3=0.95$) and later the X-polarized modes having smaller gains ($\gamma_2=0.9$, $\gamma_1=0.85$). For moderate values of p, all four modes coexist in a stable state. A subsequent increase of the pump rate p leads to the death of the mode I_1. That mode has the smallest gain, and it loses the concurrence with other modes.

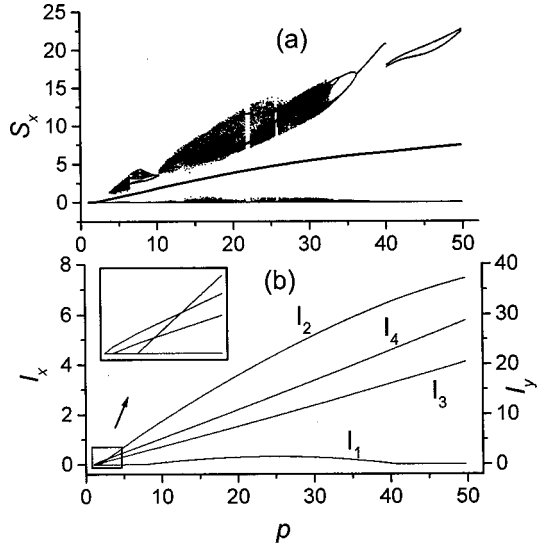

FIG. 13. (a) The minima of the intensity S_x and (b) stabilized intensities I_k as a function of the pump rate p for the mode configuration (2,2) at different values of the signal gain: $\gamma_1=0.85$, $\gamma_2=0.9$, $\gamma_3=0.95$, and $\gamma_4=1$. The thick solid line (a) corresponds to the stabilized steady state obtained by the tracking procedure. The insert (b) shows an enlarged region close to the origin.

In order to prevent spurious stable steady states that may stem from a finite-precision arithmetic, small noise was added to the system during our simulations. Uncorrelated random numbers uniformly distributed inside the interval $[0,a_n]$ with $a_n=10^{-7}$ have been added to the intensities I_k at every step of the numerical integration. The tracking procedure still worked, when the noise amplitude a_n was enlarged up to 10^{-4}. This finding clearly shows that the feedback signal can maintain the stability of the steady state, even in the presence of rather large noise.

VIII. CONCLUSIONS

The theoretical analysis of the multimode, intracavity-doubled Nd:YAG laser uncovers that unwanted chaotic regimes can be successfully stabilized by modulating the laser pump rate with the feedback signal composed of two experimentally available quantities, namely, the total intensities of the infrared light polarized in two different orthogonal directions. Our analysis is based on the model consideration of $2(m+n)$ coupled rate equations for the intensities and gains of m modes polarized in the X direction and n modes polarized in the Y direction. The stability of the steady state mainly derives from a closed system of two second-order coupled linear differential equations for the total intensities s_x and s_y that splits off from the original linearized system of the model equations. Due to this fact, the total intensities s_x and s_y are efficient feedback parameters, capable to control the stability of the fixed point.

We have analyzed different strategies based on proportional feedback control, derivative control, and combined control. In appropriate parameter spaces, we determined the stability domains of the steady state. The proportional feedback control turns out to be most convenient for experimental applications. For this control strategy, we derived ap-

proximate analytical conditions of stability.

The linear control theory has been verified numerically by simulating the original model of $2(m+n)$ nonlinear coupled differential equations. Therefore, it follows that the fixed point of the controlled system has only a finite domain of attraction. The trajectories lying on the strange attractor of the system are far away from the fixed point and, hence, cannot be stabilized by simply switching on the feedback perturbation. Stabilization of the system, however, can be attained via the tracking procedure. We have analyzed a modified proportional feedback technique that incorporates a low-pass filter into the feedback loop, in order to provide an automatic adjustment to the position of the fixed point. We also have investigated numerically the influence of scattering of the parameters of different modes as well as the influence of noise. Our theoretical analysis strongly proves that the above chaos control method is applicable to a real-world laser experiment.

ACKNOWLEDGMENTS

The authors would like to thank H. Kantz, E. Sinde, U. Dreßler, A. Schenck zu Schweinsberg, M. Bünner, W. Just, and R. Meitzner for fruitful collaborations. The present work was supported financially by the Max-Planck-Gesellschaft and the Bundesministerium für Bildung, Wissenschaft, Forschung und Technologie (BMBF) under Contract No. 13N7036.

[1] J. Baer, J. Opt. Soc. Am. B **3**, 1175 (1986).
[2] P. Mandel and X.-G. Wu, J. Opt. Soc. Am. B **3**, 940 (1986); X.-G. Wu and P. Mandel, *ibid.* **4**, 1870 (1987).
[3] M. Oka and S. Kubota, Opt. Lett. **13**, 805 (1988).
[4] G. E. James, E. M. Harrel, II, C. Bracikowski, K. Wiesenfeld, and R. Roy, Opt. Lett. **15**, 1141 (1990).
[5] C. Bracikowski and R. Roy, Chaos **1**, 49 (1991).
[6] C. Liu, R. Roy, H. D. I. Abarbanel, Z. Gills, and K. Nunes, Phys. Rev. E **55**, 6483 (1997).
[7] P. Colet, R. Roy, and K. Wiesenfeld, Phys. Rev. E **50**, 3453 (1994).
[8] E. R. Hunt, Phys. Rev. Lett. **67**, 1953 (1991).
[9] S. Bielawski, M. Bouazaoui, D. Derozier, and P. Glorieux, Phys. Rev. A **47**, 3276 (1993).
[10] K. Ogata, *Modern Control Engineering* (Prentice Hall, Englewood Cliffs, NJ, 1990).
[11] W. H. Press, B. P. Flannery, S. A. Teukolsky, and W. T. Vetterling, *Numerical Recipes in C: the Art of Scientific Computing* (Cambridge University Press, Cambridge, 1992).
[12] A. Namajūnas, K. Pyragas, and A. Tamaševičius, Phys. Lett. A **204**, 255 (1995).